Volume 1 | Number 1 | Jan 2013 | Pages 1–100

Nanoscale

www.rsc.org/nanoscale

ROYAL SOCIETY
OF CHEMISTRY

ROYAL SOCIETY
OF CHEMISTRY

www.rsc.org/nanoscale

A novel and promising ozone gas sensor based on α-Ag$_2$WO$_4$ rod-like structures are obtained via a microwave-assisted hydrothermal method. The electrical resistance measurements show a good gas sensor performance of nanorods at operating temperature of 300°C, especially a fast response and short recovery time.
254x203mm (96 x 96 DPI)

Journal Name

COMMUNICATION

A novel ozone gas sensor based on one-dimensional (1D) α-Ag₂WO₄ nanostructures

Luís. F. da Silva,*[a] Ariadne C. Catto,[b] Waldir Avansi Jr,[c] Laécio S. Cavalcante,[d] Juan Andrés,[e] Khalifa Aguir,[f] Valmor R. Mastelaro [b] and Elson Longo[a]

This paper reports on a new ozone gas sensor based on α-Ag₂WO₄ nanorod-like structures. Electrical resistance measurements proved the efficiency of α-Ag₂WO₄ nanorods, which rendered a good sensitivity even for a low ozone concentration (80 ppb), a fast response and short recovery time at 300°C, demonstrating great potential for a variety of applications.

Metal semiconducting oxides have drawn the interest of many researchers due to their wide range of applications, especially as gas sensing materials. [1-5] Among them, one-dimensional (1-D) semiconductor nanostructures have been proposed as very interesting materials, especially as gas sensor devices. [6-12] It is well known that several technological applications of nanostructured materials are directly related to the morphology, particle size, crystalline phase and activity of specific crystalline planes strictly dependent on synthesis methods. [4, 13-15] In particular, the relationship between morphology and gas sensing properties has been well stablished. [4,16,17]

Tungsten-based oxides are an important class of materials that display wide potential functional properties,[18-20] specifically the silver tungstate (Ag₂WO₄) compound, which can exhibit three different structures: α–orthorhombic, β–hexagonal, and γ–cubic.[21-25] Recently, our research group reported a detailed study of the synthesis, structural and optical properties of hexagonal nanorod-like elongated α-Ag₂WO₄ nanocrystals obtained by different methods.[26-28]

Ozone (O₃) is an oxidizing gas used in many technological applications in different areas, such as food industry, drinking-water treatment, medicine, microelectronic cleaning processes, and others.

[29, 34-39] For example, ozone has been employed as a powerful drinking-water disinfectant and oxidant. [34, 35, 40] On the other hand, when the ozone level in an atmosphere exceeds a certain threshold value, the exposure to this gas becomes hazardous to human health and can cause serious health problems (e.g. headache, burning eyes, respiratory irritation and lung damage).[34, 41] The European Guidelines (2002/3/EG) recommend avoiding exposure to ozone levels above 120 ppb.[41] Such arguments support the requirement for the determination and continuous monitoring of ozone levels.[3, 29, 41]

Gas sensing properties are evaluated in terms of operating temperature, sensitivity, response time, recovery time and stability. [29-33] SnO₂, In₂O₃ and WO₃ compounds have been considered the most promising ozone gas sensors.[29-33]

To the best of our knowledge, to date the gas sensing properties of α-Ag₂WO₄ nanocrystals have never been evaluated.

Here, we report the sensing properties of 1-D α-Ag₂WO₄ nanorod-like structures obtained by the microwave-assisted hydrothermal (MAH) method. Because of such properties, nanorods are potential candidates for practical applications as ozone gas sensors.

The crystalline phase of the as-obtained α-Ag₂WO₄ sample was analyzed by x-ray diffraction measurement and all reflections were indexed to an orthorhombic structure with a *Pn2n* space group (ICSD file No. 4165) with no secondary phases (see Fig. S1 in the ESI).

The FE-SEM and TEM images in Fig. 1 show that the α-Ag₂WO₄ crystals exhibit a one-dimensional (1D) and uniform morphology composed of 100 nm wide nanorods. The one-dimensional nature observed for the as-prepared nanostructures is related to the preferential growth in the [001] direction.[27, 28] Additionally, the α-Ag₂WO₄ nanorods exhibit other nanoparticles on

their surface. Recently, we reported the real-time *in situ* observation of the silver metallic (Ag) growth process from the unstable α–Ag$_2$WO$_4$ nanorods submitted to an electron irradiation from a transmission electron microscopy.[27, 28] Nevertheless, we must emphasize that the α–Ag$_2$WO$_4$ nanorods used in the ozone sensor measurements were not exposed to electron irradiation, and consequently, Ag nanoparticles are not present on the α–Ag$_2$WO$_4$ nanorods' surface.
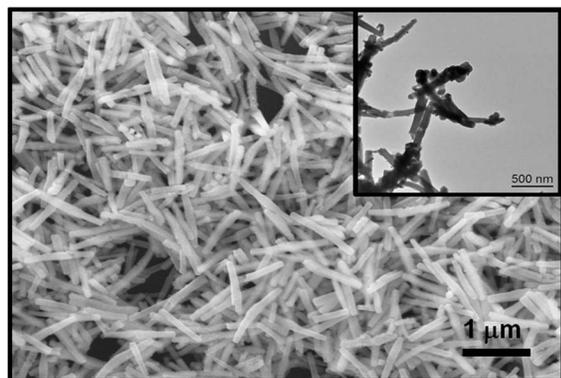

Fig. 1   FE-SEM image of the α-Ag$_2$WO$_4$ nanorods. The inset shows a TEM image of the nanorods.

The resistance response of the α-Ag$_2$WO$_4$ nanorods was studied at an operating temperature of 300°C under the exposure of 500 ppb of ozone gas at different times (15, 30 and 60 s) and the results are depicted in Fig. 2. The electrical resistance response is typical of an *n*-type semiconductor material exposed to oxidizing gases. The oxygen species (O$_2^-$ and O$^-$) chemisorbed onto the semiconductor surface decrease the conductivity of the sensor device due to the lower concentration of free electrons in the conduction band.[29, 33] It is noteworthy that the α-Ag$_2$WO$_4$ nanorods display good sensitivity, a fast response as well as short recovery time (Table 1).
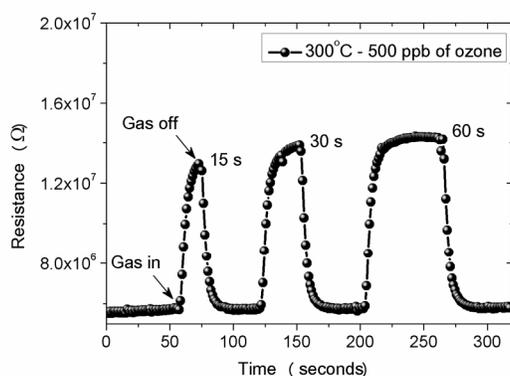

Fig. 2   Ozone gas sensing response for α-Ag$_2$WO$_4$ nanorods upon exposure to differing times at operating temperature of 300°C. Arrows indicate when the ozone gas flow was turned on and off.

As can be seen in Fig.2, the sample also exhibits good sensitivity to the different exposure times as well as total reversibility and good stability of the base line.

Fig. 3(a) shows the ozone gas sensing performance of α-Ag$_2$WO$_4$ nanorods at different operating temperatures (300°C and 350°C) and different ozone concentrations. For both operating temperatures, the sensitivity increases with ozone concentration and greater sensitivity is observed at 300°C, considered the best operating temperature. The ozone gas responses of α-Ag$_2$WO$_4$ nanorods at 300°C and 350°C upon exposure to different gas concentrations are displayed in Figs.S2 and S3 (ESI).
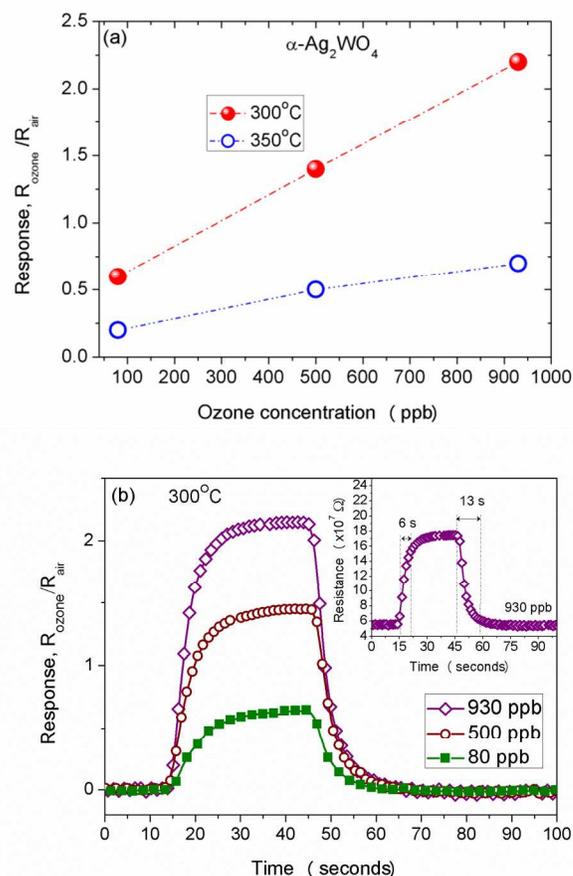

Fig. 3   Response dependence on the ozone concentration of α-Ag$_2$WO$_4$ nanorods (a) at an operating temperature of 300°C and 350°C. (b) Ozone gas sensor response at 300°C. Inset shows the response and recovery time for 930 ppb of ozone.

The ozone sensitivity of α-Ag$_2$WO$_4$ nanorods operating at 300°C and exposed to a range of ozone concentration from 80 to 930 ppb was also evaluated and the results are shown in Fig. 3(b). The α-Ag$_2$WO$_4$ nanorod-based sensor displayed good sensitivity and no evidence of saturation in the concentration range evaluated. As can be seen in Table 1, even at a low concentration (80 ppb), they exhibit fast response time of 7 s and short recovery time of 13 s, similarly to the results for high concentrations of ozone.

For comparison, Table 1 also shows the results reported for WO$_3$-, In$_2$O$_3$- and SnO$_2$- based ozone gas sensors.[29, 31, 33] An analysis of the results has revealed that the operating temperature of α-Ag$_2$WO$_4$-based sensor is close to that of WO$_3$, In$_2$O$_3$ and SnO$_2$ materials and the response time is slightly larger than that of WO$_3$-
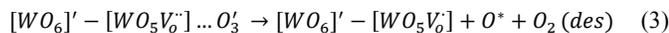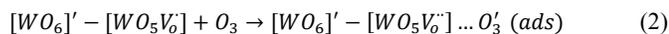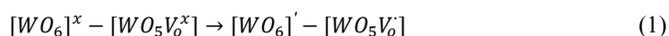
Nanoscale Accepted Manuscript

and SnO$_2$- based sensors, but significantly shorter than that of In$_2$O$_3$-based sensors. On the other hand, the recovery time of α-Ag$_2$WO$_4$-based sensor is shorter than that of WO$_3$-, In$_2$O$_3$- and SnO$_2$- based sensors.

Table 1 Comparison of the parameters of ozone gas sensing properties of α-Ag$_2$WO$_4$ sample and WO$_3$-, In$_2$O$_3$-, and SnO$_2$-based chemiresistors.
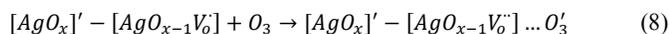
Sensor	Operating Temp. (^{o}C)	Ozone level (ppb)	Response time (s)	Recovery time (s)	Reference
WO$_3$	250	80	1	60	[33]
In$_2$O$_3$	300	100	60	6000	[31]
SnO$_2$	250	1000	2	1000	[29]
Ag$_2$WO$_4$	300	930	6	16	This study
Ag$_2$WO$_4$	300	500	7	14	This study
Ag$_2$WO$_4$	300	80	7	13	This study

We can propose two effects of O$_3$ adsorption in the α-Ag$_2$WO$_4$ sample. The α-Ag$_2$WO$_4$ crystals have an orthorhombic structure and distorted [WO$_6$] clusters with an octahedral configuration, therefore, the α-Ag$_2$WO$_4$ orthorhombic structure has four different types of coordination for the Ag$^+$ ion and six possible configurations for the [AgO$_x$] x= 2, 4, 6 or 7 clusters. For the tetrahedral [AgO$_4$] and deltahedral [AgO$_7$] clusters, there are two possible configurations, as shown by the different bonds, distances and angles. [26-28] The first effect is intrinsic to that of the sample and the second is a consequence of the surface and interface complex cluster defects which produce extrinsic defects. Before the adsorption of O$_3$, the short and medium range order structural defects generate non-homogeneous charge distribution in the cell. After the O$_3$ adsorption, the configuration charges and distorted excited clusters are formed, allowing electrons to become trapped (O$_3$'). Therefore the gas sensing mechanism can be described according to the following equations:

The first effect,

$$[WO_6]^x - [WO_5V_o^x] \rightarrow [WO_6]' - [WO_5V_o^{\cdot}] \tag{1}$$

$$[WO_6]' - [WO_5V_o^{\cdot}] + O_3 \rightarrow [WO_6]' - [WO_5V_o^{\cdot\cdot}]...O_3' \ (ads) \tag{2}$$

$$[WO_6]' - [WO_5V_o^{\cdot\cdot}]...O_3' \rightarrow [WO_6]' - [WO_5V_o^{\cdot}] + O^* + O_2 \ (des) \tag{3}$$

The second effect,

$$[WO_6]_o^x - [WO_5]_d^x \rightarrow [WO_6]_o' - [WO_5]_d^{\cdot} \tag{4}$$

$$[WO_6]_o' - [WO_5]_d^{\cdot} + O_3 \rightarrow [WO_6]_o^x - [WO_5]_d^{\cdot}...O_3' \ (ads) \tag{5}$$

$$[WO_6]_o^x - [WO_5]_d^{\cdot}...O_3' \rightarrow [WO_6]_o^x - [WO_5]_d^x + O^* + O_2 \ (des) \tag{6}$$

$$[AgO_x]^x - [AgO_{x-1}V_o^x] \rightarrow [AgO_x]' - [AgO_{x-1}V_o^{\cdot}] \tag{7}$$

$$[AgO_x]' - [AgO_{x-1}V_o^{\cdot}] + O_3 \rightarrow [AgO_x]' - [AgO_{x-1}V_o^{\cdot\cdot}]...O_3' \tag{8}$$

$$[AgO_x]' - [AgO_{x-1}V_o^{\cdot\cdot}]...O_3' \rightarrow [AgO_x] - [AgO_{x-1}V_o^{\cdot}] + O^* + O_2 \ (des) \tag{9}$$
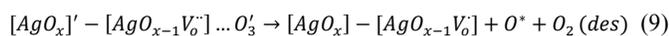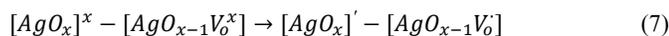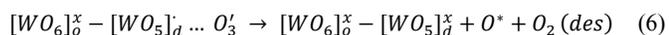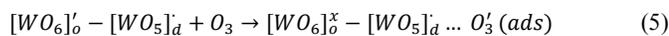
Conclusions

The α-Ag$_2$WO$_4$ nanorod-like structures obtained via MAH route were evaluated as promising ozone sensors. They have shown great potential as novel ozone gas sensors and displayed good sensitivity to low ozone concentrations as well as good stability, a fast response and short recovery time.

Experimental Section

Preparation of α-Ag$_2$WO$_4$ nanorods

An α–Ag$_2$WO$_4$ powder was prepared at 160ºC for 1 h with 1 g of PVP40 ((C$_6$H$_9$NO)$_n$; 99%) by the MAH method. All reagents were obtained from Aldrich company. The typical α–Ag$_2$WO$_4$ sample synthesis procedure is described as follows: 1 mM of Na$_2$WO$_4$.2H$_2$O (99.5%) and 2 mM of AgNO$_3$ (99.8%) were separately dissolved with deionized water contained in two plastic tubes of 50 mL each. Before the dissolution of the salts, 0.5 g of polymer surfactant (PVP40) was dissolved in both tubes. 100 mL of the suspension were transferred to a Teflon vessel autoclave. The Teflon reactor was then sealed, placed inside an adapted domestic microwave system and processed for 1h at 160ºC. The resulting suspension was washed with deionized water several times for the removal of the remaining Na$^+$ ions and organic compounds. Finally, a light beige powdered precipitate was collected and dried with acetone for 6 h at room temperature.

Structural and morphological characterization

The sample was structurally characterized by x-ray diffraction (XRD) using CuKα radiation (Rigaku diffractometer, model D/Max-2500PC) in a 2θ range from 10° to 70° with a step of 0.02^o at a scanning speed of 2°.min^{-1}. The morphology of the as-obtained sample was studied by transmission electron microscopy (TEM) on a JEM 2010 URP operating at 200 kV and by field emission scanning electron microscopy (FE-SEM) on a Zeiss Supra35 operating at 5 kV.

Gas sensor preparation

The α-Ag$_2$WO$_4$ powders were dispersed in isopropyl alcohol by an ultrasonic cleaner for 30 minutes and the suspension was then dripped onto a SiO$_2$/Si substrate containing 100-nm thick Pt electrodes separated by a distance of 50 μm. The sample was heat-treated for 2 hours at 500°C in an electric furnace under air atmosphere.

Ozone gas sensor measurements

The sensor sample was inserted into a test chamber for the control of the temperature under different ozone concentrations. The ozone gas was formed from the oxidizing of oxygen molecules of dry air (8.3 cm^3.s^{-1}) by a calibrated pen-ray UV lamp (UVP, model P/N 90-0004-01) and provided ozone concentrations from 80 to 930 ppb. The dry air containing ozone was blown directly onto the sensor

placed on a heated holder. The *dc* voltage applied was 1 V while the electrical resistance was measured by a Keithley (model 6514) electrometer. The response (S) was defined as $S = R_{ozone}/R_{air}$, where R_{ozone} and R_{air} are the electric resistances of the sensor exposed to ozone gas and dry air, respectively.

The response time of the sensor was defined as the time required for a change in the sample's electrical resistance to reach 90% of the initial value when exposed to ozone gas. Similarly, the recovery time was defined as the time required for the electrical resistance of the sensor to reach 90% of the initial value after the ozone gas has been turned off.

Acknowledgements

Notes and references

a LIEC, Instituto de Química, Universidade Estadual Paulista, P.O. Box 355, 14800-900, Araraquara, SP, Brazil, Tel: +55 16 33016643
*E-mail: lfsilva83@gmail.com

b Instituto de Física de São Carlos, Universidade de São Paulo, Avenida Trabalhador São-carlense, 400, 13566-590, São Carlos, SP, Brazil. Tel: +55 16 33739828

c Departamento de Física, Universidade Federal de São Carlos, Rodovia Washington Luiz, km 235, 13565-905, São Carlos, SP, Brazil

d Departamento de Química, Universidade Estadual do Piauí, 64002-150, Teresina, PI, Brazil

e Departamento Química-Física y Analítica, Universitat Jaume I, Campus de Riu Sec, Castelló E-12080, Spain

f Aix Marseille Université, CNRS IM2NP (UMR 7334), FS St Jérôme S152, Marseille, 13397, France

† Electronic Supplementary Information (ESI) available: [The x-ray diffraction pattern, and ozone gas sensor response at an operating temperature of 300ºC and 350ºC]. See DOI: 10.1039/c000000x/

1. X. Chen, C. K. Y. Wong, C. A. Yuan and G. Zhang, *Sens. Actuators, B* 2013, **177**, 178-195.
2. E. Comini, C. Baratto, I. Concina, G. Faglia, M. Falasconi, M. Ferroni, V. Galstyan, E. Gobbi, A. Ponzoni, A. Vomiero, D. Zappa, V. Sberveglieri and G. Sberveglieri, *Sens. Actuators, B* 2013, **179**, 3-20.
3. V. R. Mastelaro, S. C. Zílio, L. F. da Silva, P. I. Pelissari, M. I. B. Bernardi, J. Guerin and K. Aguir, *Sens. Actuators, B* 2013, **181**, 919-924.
4. D. P. Volanti, A. A. Felix, M. O. Orlandi, G. Whitfield, D. J. Yang, E. Longo, H. L. Tuller and J. A. Varela, *Adv. Funct. Mater.* 2013, **23**, 1759-1766.
5. E. Rossinyol, J. Arbiol, F. Peiró, A. Cornet, J. R. Morante, B. Tian, T. Bo and D. Zhao, *Sens. Actuators, B* 2005, **109**, 57-63.
6. E. Comini, *Anal. Chim. Acta* 2006, **568**, 28-40.
7. M. Sarikaya, C. Tamerler, D. T. Schwartz and F. Baneyx, *Annu. Rev. Mater. Res.*, 2004, **34**, 373-408.
8. A. Kolmakov and M. Moskovits, *Annu. Rev. Mater. Res.* 2004, **34**, 151-180.
9. M. E. Franke, T. J. Koplin and U. Simon, *Small* 2006, **2**, 301-301.
10. Y. Cui, Q. Q. Wei, H. K. Park and C. M. Lieber, *Science* 2001, **293**, 1289-1292.
11. G. Shen, P.-C. Chen, K. Ryu and C. Zhou, *J. Mater. Chem.* 2009, **19**, 828-839.
12. K. J. Choi and H. W. Jang, *Sensors*, 2010, **10**, 4083-4099.
13. H. Mourao, A. R. Malagutti and C. Ribeiro, *Appl. Catal., A* 2010, **382**, 284-292.
14. G. Korotcenkov, *Mater. Sci. Eng. Rep.*, 2008, **61**, 1-39.
15. L. F. da Silva, W. Avansi, M. L. Moreira, A. Mesquita, L. J. Q. Maia, J. Andres, E. Longo and V. R. Mastelaro, *J. Nanomater.* 2012, **2012**, 890397.
16. M. R. Alenezi, S. J. Henley, N. G. Emerson and S. R. Silva, *Nanoscale* 2014, **6**, 235-247.
17. M. M. Arafat, B. Dinan, S. A. Akbar and A. S. M. A. Haseeb, *Sensors* 2012, **12**, 7207-7258.
18. S.-H. Yu, B. Liu, M. –S. Mo, J.-H. Huang, X. –M. Liu and Y. –T. Qian, *Adv. Func. Mater.* 2003, **13**, 639-647.
19. P. Hu and Y. Cao, *Dalton Trans.* 2012, **41**, 8908-8912.
20. S. -H. Yu, M. Antonietti, H. Cölfen and M. Giersig, *Angew. Chem. Int. Ed.* 2002, **41**, 2356-2360.
21. A. J. Vandenberg and C. A. H. Juffermans, *J. Appl. Crystallogr.* 1982, **15**, 114-116.
22. Q. P. Wang, X. X. Guo, W. H. Wu and S. X. Liu, in *Mater. Des., Pts 1-3* (Eds: X. M. Sang, P. C. Wang, L. Ai, Y. G. Li and J. L. Bu) 2011, Vol. **284-286**, pp. 1321-1325.
23. R. R. Kharade, S. S. Mali, S. P. Patil, K. R. Patil, M. G. Gang, P. S. Patil, J. H. Kim and P. N. Bhosale, *Electrochim. Acta* 2013, **102**, 358-368.
24. L. Pan, L. Li and Y. H. Chen, *J. Sol-Gel Sci. Technol.* 2013, **66**, 330-336.
25. J. Tang and J. Ye, *J. Mater. Chem.* 2005, **15**, 4246-4251.
26. L. S. Cavalcante, M. A. P. Almeida, W. Avansi, R. L. Tranquilin, E. Longo, N. C. Batista, V. R. Mastelaro and M. S. Li, *Inorg. Chem.* 2012, **51**, 10675-10687.
27. E. Longo, L. S. Cavalcante, D. P. Volanti, A. F. Gouveia, V. M. Longo, J. A. Varela, M. O. Orlandi and J. Andres, *Sci. Rep.* 2013, **3**, 1676.
28. E. Longo, D. P. Volanti, V. M. Longo, L. Gracia, I. C. Nogueira, M. A. P. Almeida, A. N. Pinheiro, M. M. Ferrer, L. S. Cavalcante and J. Andrés, *J. Phys. Chem. C* 2014, DOI: 10.1021/jp408167v.
29. G. Korotcenkov and B. K. Cho, *Sens. Actuators, B* 2012, **161**, 28-44.
30. G. Korotcenkov, I. Blinov, M. Ivanov and J. R. Stetter, *Sens. Actuators, B* 2007, **120**, 679-686.
31. M. Epifani, S. Capone, R. Rella, P. Siciliano, L. Vasanelli, G. Faglia, P. Nelli and G. Sberveglieri, *J. Sol-Gel Sci. Technol.* 2003, **26**, 741-744.
32. K. Aguir, C. Lemire and D. B. B. Lollman, *Sens. Actuators, B* 2002, **84**, 1-5.

33. M. Bendahan, R. Boulmani, J. L. Seguin and K. Aguir, *Sens. Actuators, B* 2004, **100**, 320-324.

34. L. C. Simoes and M. Simoes, *RSC Adv.* 2013, **3**, 2520-2533.

35. W. H. Glaze, *Environ. Sci. Technol.* 1987, **21**, 224-230.

36. B. Clavo, D. Ceballos, D. Gutierrez, G. Rovira, G. Suarez, L. Lopez, B. Pinar, A. Cabezon, V. Morales, E. Oliva, D. Fiuza and N. Santana-Rodriguez, *J. Pain Symptom Manage.* 2013, **46**, 106-112.

37. V. Bocci, I. Zanardi and V. Travagli, *Am. J. Cardiovasc. Drugs* 2011, **11**, 73-82.

38. D. M. Graham, C. D. Sopher, R. G. Rice and A. E. Yousef, *Food Technol.* 2013, **67**, 83-84.

39. S. Patil, P. Bourke, J. M. Frias, B. K. Tiwari and P. J. Cullen, *Innovative Food Sci. Emerging Technol.* 2009, **10**, 551-557.

40. H. P. Kaiser, O. Koster, M. Gresch, P. M. J. Perisset, P. Jaggi, E. Salhi and U. von Gunten, *Ozone: Sci. Eng.* 2013, **35**, 168-185.

41. C. Y. Wang, R. W. Becker, T. Passow, W. Pletschen, K. Köhler, V. Cimalla and O. Ambacher, *Sens. Actuators, B* 2011, **152**, 235-240.

42. I. Bilecka and M. Niederberger, *Nanoscale*, 2010, **2**, 1358-1374.

43. M. Baghbanzadeh, L. Carbone, P. D. Cozzoli and C. O. Kappe, *Angew. Chem., Int. Ed.* 2011, **50**, 11312-11359.

44. M. L. Moreira, G. P. Mambrini, D. P. Volanti, E. R. Leite, M. O. Orlandi, P. S. Pizani, V. R. Mastelaro, C. O. Paiva-Santos, E. Longo and J. A. Varela, *Chem. Mater.* 2008, **20**, 5381-5387.

45. L. F. da Silva, W. Avansi, J. Andres, C. Ribeiro, M. L. Moreira, E. Longo and V. R. Mastelaro, *Phys. Chem. Chem. Phys.* 2013, **15**, 12386-12393.

46. G. A. Tompsett, W. C. Conner and K. S. Yngvesson, *Chemphyschem*, 2006, **7**, 296-319.